

## Method for analyzing $E \times B$ probe spectra from Hall thruster plumes

Rohit Shastry,<sup>1</sup> Richard R. Hofer,<sup>1</sup> Bryan M. Reid,<sup>2</sup> and Alec D. Gallimore<sup>2</sup>

<sup>1</sup>*Jet Propulsion Laboratory, California Institute of Technology, Pasadena, California 91109, USA*

<sup>2</sup>*Plasmadynamics and Electric Propulsion Laboratory, University of Michigan, Ann Arbor, Michigan 48109, USA*

(Received 3 March 2009; accepted 16 May 2009; published online 22 June 2009)

Various methods for accurately determining ion species' current fractions using  $E \times B$  probes in Hall thruster plumes are investigated. The effects of peak broadening and charge exchange on the calculated values of current fractions are quantified in order to determine the importance of accounting for them in the analysis. It is shown that both peak broadening and charge exchange have a significant effect on the calculated current fractions over a variety of operating conditions, especially at operating pressures exceeding  $10^{-5}$  torr. However, these effects can be accounted for using a simple approximation for the velocity distribution function and a one-dimensional charge exchange correction model. In order to keep plume attenuation from charge exchange below 30%, it is recommended that  $p\zeta \leq 2$ , where  $p$  is the measured facility pressure in units of  $10^{-5}$  torr and  $\zeta$  is the distance from the thruster exit plane to the probe inlet in meters. The spatial variation of the current fractions in the plume of a Hall thruster and the error induced from taking a single-point measurement are also briefly discussed. © 2009 American Institute of Physics.

[DOI: [10.1063/1.3152218](https://doi.org/10.1063/1.3152218)]

### I. INTRODUCTION

Performance and efficiency are important fundamental quantities in characterizing a Hall thruster and can require a large array of diagnostics to properly determine. While it has been shown that the majority of ions created in Hall thrusters consist of singly charged xenon ( $Xe^+$ ),<sup>1-3</sup> knowledge of the ion species' population is necessary to understand the competing processes affecting overall efficiency.<sup>4,5</sup> This population is typically measured using an  $E \times B$  probe, which acts as an ion velocity filter. Since ion velocities in the plume are proportional to charge state, an  $E \times B$  probe can differentiate between charge states and species fractions can be determined from the amount of current the probe collects at each velocity. This diagnostic has been used successfully in the past on a variety of plasma sources.<sup>1,2,4,6-8</sup> However, analysis of probe spectra from Hall thrusters is not straightforward due to the broadening and blending of current peaks associated with each ion species. These features are caused by elastic collisions within the plume as well as a range of ion acceleration voltages within the channel, phenomena which are either less prominent or absent in gridded ion thrusters. Furthermore, the high current densities associated with Hall thrusters typically results in higher facility operating pressures than ion thrusters. This results in larger amounts of charge exchange (CEX) occurring within the plume, which affects  $E \times B$  probe measurements typically performed far downstream of the thruster exit plane. Lastly, measurement of species population often relies on a single-point measurement done at thruster centerline, despite studies which show that this population varies within the plume.<sup>1,9</sup> All of these factors can result in an inaccurate determination of ion species' population in a Hall thruster plume.

The purpose of this study is to quantify the importance

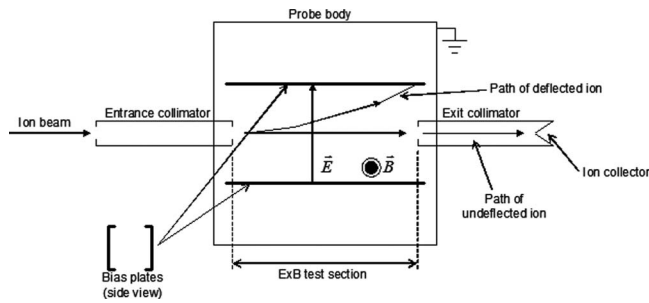
of including the above factors in determining current and species fractions in Hall thrusters. Various levels of correcting for species peak widths as well as CEX collisions were applied to  $E \times B$  probe spectra from a 6 kW laboratory Hall thruster. The results from these methods were then compared to characterize the importance of correcting for the above factors. An analysis method is then recommended which is shown to provide the best balance between simplicity and accuracy.

The paper is organized as follows: Sec. II describes the experimental apparatus used to collect  $E \times B$  spectra over a wide range of operating conditions. Section III illustrates the four methods studied to account for species peak width. Section IV details the model used to correct for CEX along with numerous simplifications and their validation. Section V gives the results of the comparison between analysis methods for several pertinent operating conditions. Section VI summarizes the results and provides recommendations based on them, discusses uncertainty generated by the additional analysis required in these methods, and addresses the issue of spatial variation of species fraction within the plume. Finally, Sec. VII gives the conclusions and recommendations of the study.

### II. EXPERIMENTAL APPARATUS

#### A. $E \times B$ probe

An  $E \times B$  probe or Wien filter is a bandpass ion filter that selects ions according to their velocities through the application of crossed electric and magnetic fields.<sup>1,2,4,6-8,10</sup> Most probes establish a constant magnetic field with permanent magnets while the electric field is established between two parallel plates. Sweeping the plate voltage while monitoring the ion current that passes through the probe yields a current-

FIG. 1. Schematic of  $E \times B$  probe. Note: not to scale.

voltage characteristic that is related to the ion velocity distribution function. Because the velocity of multiply charged ions in Hall thrusters is proportional to the square root of their charge state, an  $E \times B$  probe can be used to discriminate between ion species. Analysis of the ion current from the probe characteristic can then be used to compute the ion species fractions.

As shown in Fig. 1, the  $E \times B$  probe is made up of three main sections: the entrance collimator,  $E \times B$  test section, and exit collimator. Ions passing through the entrance collimator must travel through the test section undeflected to reach the collector. The motion of an ion through the test section is described by the Lorentz force equation given by

$$\vec{F} = eZ(\vec{E} + \vec{u} \times \vec{B}). \quad (1)$$

The test section filters particles with a particular velocity by balancing the electric and magnetic fields such that there is no net force acting on those particles. Permanent magnets are usually employed to establish a constant magnetic field while the electric field is typically established between two parallel plates separated by a gap distance  $d$  and biased to a potential  $V_{\text{probe}}$ . Setting the force equal to zero in Eq. (1), the velocity of an ion passing through the test section undeflected is

$$u_{\text{pass}} = \frac{E}{B} = \frac{V_{\text{probe}}}{Bd}. \quad (2)$$

Since the gap distance and magnetic field are fixed, the ion velocity is proportional to the probe voltage. Thus, the probe voltage can be swept across an appropriate range to capture the current from various charge states. The current collected at any given voltage can be written as

$$I_i = eZ_i n_i u_i A_c = eZ_i n_i \sqrt{\frac{2eZ_i V_{a,i}}{m_{Xe}}} A_c, \quad (3)$$

where  $Z_i$  is the ion's charge state,  $n_i$  is the number density,  $V_{a,i}$  is the ion's acceleration voltage, and  $A_c$  is the probe collection area. The second term assumes the ions were accelerated electrostatically through potential  $V_{a,i}$ . Secondary electron emission effects are not included in this particular analysis as in Ref. 4 because of the use of a specially shaped collector that recollects any secondary emission current. However, these effects involve only a minor correction as the secondary electron yields are low for typical xenon energies incident on tungsten.<sup>4</sup> Once currents from each species are measured, they can be used to determine their respective current fractions defined as

$$\Omega_i = \frac{I_i}{\sum I_i} = \frac{n_i Z_i^{3/2}}{\sum n_i Z_i^{3/2}}. \quad (4)$$

The second term neglects the variation in acceleration voltage across species as they tend to only differ by a few tens of volts.<sup>4</sup> Noting that the denominator in Eq. (4) is a normalization factor, it can be inverted to determine the corresponding species fractions given by

$$\zeta_i = \frac{n_i}{\sum n_i} = \frac{\Omega_i / Z_i^{3/2}}{\sum \Omega_i / Z_i^{3/2}}. \quad (5)$$

The  $E \times B$  probe used in these experiments was used previously during the NSTAR extended life test at the Jet Propulsion Laboratory (JPL).<sup>11</sup> The probe was positioned 1.9 m downstream of the thruster exit plane on thruster centerline. The entrance collimator was 13.4 cm in length and had two circular orifices at either end that were 0.027 cm in diameter. In the 12.7-cm-long test section, the magnetic field was applied with permanent magnets that provided a magnetic field strength at the test section center of 0.1 T. The electric field was established with a pair of aluminum plates machined from channel stock. The bias plates were separated by a distance of  $d = 1.9$  cm with legs used to minimize electric field fringing that were  $d/4$  in length.<sup>10</sup> The exit collimator was 4 cm long and had an entrance orifice diameter of 0.027 cm. A high-aspect-ratio concave-shaped tungsten collection electrode was placed at the end of the exit collimator. The concave shape was chosen so that secondary electrons emitted from the collector would be recaptured. The acceptance angle of the probe was less than  $0.1^\circ$ . Probe resolution was conservatively estimated as 0.5% of the ion energy.

## B. Faraday probe

Surveys of the ion current density in the thruster plume were taken using a Faraday probe. The probe consisted of a 1.9-cm-diameter collection electrode enclosed within a 2.5-cm-diameter guard ring. The guard ring and collector were separated by a 0.1 cm gap, were fabricated from graphite and were biased  $-30$  V below facility ground to repel electrons.

## C. Vacuum facility

Experiments were performed in the Endurance Test Facility at JPL. The 3-m-diameter by 10-m-long vacuum chamber was previously used for the 30 kh life test of the 2.3 kW NSTAR ion thruster and has also been used to test the NEXIS ion thruster at power levels exceeding 20 kW.<sup>11,12</sup> The facility is cryogenically pumped and is lined with graphite panels to minimize backscattered material to thruster surfaces. Base pressures between  $10^{-8}$  and  $10^{-7}$  torr are routinely achieved. Pressure measurements were corrected for xenon using the base pressure on air and a correction factor of 2.87. For example, at a total xenon flow rate of 22.5 mg/s the operating pressure was  $1.6 \times 10^{-5}$  torr after correcting for xenon.

## D. Hall thruster

Experiments were performed using a 6 kW laboratory model Hall thruster that has an approximate throttling range of 100–500 mN thrust and 1000–3000 s specific impulse. The hollow cathode used to maintain and neutralize the discharge was mounted on the thruster centerline inside the inner magnetic core of the thruster. The cathode was always operated at 7% of the anode mass flow rate. Power and propellant were delivered to the thruster with commercially available power supplies and flow controllers. The plasma discharge was sustained by a matching pair of power supplies wired in parallel that provided a maximum output of 500 V, 40 A. The discharge filter consisted of a 40  $\mu\text{F}$  capacitor in parallel with the discharge power supply outputs. Additional power supplies were used to power the magnet coils and the cathode heater and keeper. The cathode heater and keeper were used only during the thruster ignition sequence. Research-grade xenon (99.9995% pure) was supplied through stainless steel feed lines with 50 and 500 (SCCM) (SCCM denotes standard cubic centimeters per minute at STP) mass flow controllers. The controllers were calibrated after the experiment and were digitally controlled with an accuracy of  $\pm 1\%$  of the set point.

## III. METHODS FOR DETERMINING CURRENT FRACTIONS

As mentioned in the Sec. II, current fractions for each species must be determined from the  $E \times B$  probe spectrum in order to quantify their relative populations. Determination of these fractions, however, is not straightforward due to the broadening and blending of peaks associated with each charge state. This effect is caused by a variety of factors, such as the presence of a range of acceleration voltages within the thruster (as all ions are not created in the same location), as well as collisional effects within the plume. These features are more prominent in spectra from Hall thruster plumes; spectra from ion engines contain flatter, more well-defined peaks due to their clear separation of ionization and acceleration zones, making data analysis more straightforward. The analysis of the resulting velocity distribution functions (VDFs) was performed rigorously by Kim.<sup>1</sup> However, the present study is not concerned with such detailed analyses of the measured VDFs, but rather in quantifying the importance of the VDF in calculating current and species fractions with minimal uncertainty. Motivation for including the entire peak within this calculation was suggested by Beal.<sup>13</sup> If all species are subject to the same range of acceleration voltages, then it can be shown from the electrostatic acceleration and  $E \times B$  probe equations that

$$\Delta V_{\text{probe}} \sim \Delta u \sim Z_i^{1/2}. \quad (6)$$

This indicates that the range in probe voltages induced by the range in acceleration voltages is naturally larger for higher charge states. Thus, simply neglecting this broadening by only using the peak heights to characterize each species<sup>4</sup> may introduce higher uncertainty into the calculated current fractions.

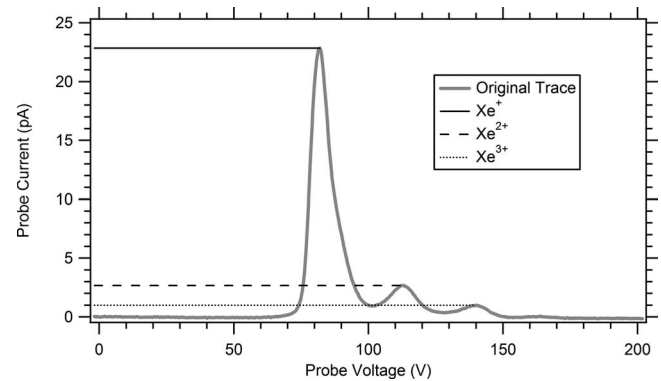


FIG. 2. Illustration of the method of peak heights.

In order to determine the importance of including the peak width in the calculation of current fractions, four different analysis methods were employed and compared: peak heights, triangle fitting, Gaussian fitting, and variable exponential fitting. A description of each of these methods can be found below.

### A. Method of peak heights

This method, suggested by Hofer,<sup>4</sup> is the simplest and most straightforward of the four investigated. Under the assumption that the variation in peak widths can be neglected, the current for each species is taken as the maximum of its corresponding peak (see Fig. 2). While this method largely ignores peak width and the overlap areas between peaks, it is attractive due to its simplicity and ease of automation.

### B. Method of triangle fitting

This method, suggested by Beal,<sup>13</sup> is a simple, first-order method to include the effects of peak broadening in current fraction determination. Triangles are effectively drawn over each peak using lines which connect the peak height and the point of half-maximum. Since the right side of each peak is typically more well-defined than the left, this line is drawn on the right side of each peak and mirrored on the left to create a symmetric triangle (see Fig. 3). The area of this triangle is then taken as the current collected for the corresponding species. It can be shown that the product of the maximum current and the half-width at half-maximum (HWHM) is proportional to the area of the full triangle.

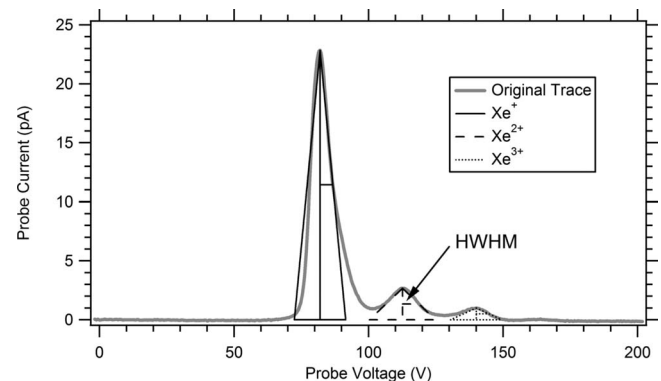


FIG. 3. Illustration of the method of triangle fitting.

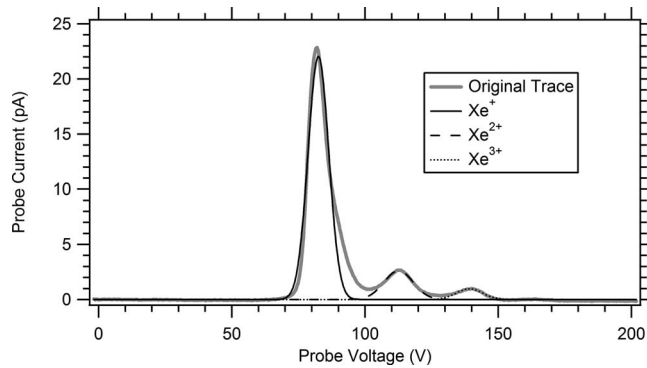


FIG. 4. Illustration of the method of Gaussian fitting.

Since these values will only be used to calculate ratios, this product is used as a measure of the collected current. While this method is only a rough measure of the total current collected for each peak, it captures a large amount of the broadening effect while remaining relatively straightforward.

### C. Method of Gaussian fitting

This method, suggested by Linnell,<sup>14</sup> is an attempt to more accurately capture the total peak for each species by fitting a symmetric Gaussian profile to them. A fit is first attempted on the highest observed charge state ( $\text{Xe}^{3+}$  in this investigation). The function is forced to approach zero at positive and negative infinity. Once a fit is found, the resulting function is then subtracted off the original  $E \times B$  probe spectrum so as not to double-count current. The process is then repeated until all peaks have fits (see Fig. 4). Each Gaussian profile is then integrated over all voltages to obtain the collected current for each species. As seen in Fig. 4, while the Gaussian fits appear to capture more of the area under each peak than the triangle fits, it fails to fully include the overlap regions between each peak.

### D. Method of variable exponential fitting

This method, proposed by Kim,<sup>1</sup> is another attempt at capturing the total peak using a functional fit. In an effort to determine a proper function to describe the spread in velocities of each species, Kim argued that the function must lie in between a Gaussian, which goes as  $e^{v^2}$  and a Druyvesteyn profile, which goes as  $e^{v^4}$ . This is because a Gaussian function describes an equilibrium distribution due to collisional processes, while a Druyvesteyn function describes a steady-state electron or ion distribution in a uniform steady electric field with elastic collisions between particles and neutral atoms. Since the velocity distribution of ions in the plume is likely created by a combination of these two, the desired function is also likely a combination of the two functions. Thus, since the only difference between these two distributions is the value of the exponent, Kim derived a fit function based on a variable exponential model, which is shown below.

Following Kim, the current collected for a given velocity  $u$  can be written as

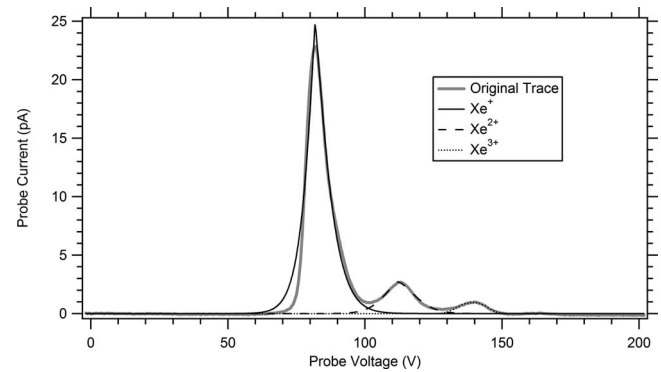


FIG. 5. Illustration of the method of variable exponential fitting.

$$I = eZnuA_c. \quad (7)$$

Given an energy distribution function  $f(E)$  or a corresponding speed distribution function  $f(C)$ , we can write

$$n \sim f(E)dE \sim f(C)dC. \quad (8)$$

Assuming that the velocity of beam ions is largely one-dimensional, then

$$u \sim C \sim V_{\text{probe}}. \quad (9)$$

Thus, given the variable exponential form for  $f(E)$ ,

$$f(E) = K * E^{1/2} * \exp(-\beta * |\sqrt{E} - \sqrt{E_b}|^n), \quad (10)$$

and that

$$E \sim C^2, \quad dE \sim CdC, \quad (11)$$

one can determine the functional form for  $I(V_{\text{probe}})$ ,

$$I = K'' * V_{\text{probe}}^3 * \exp(-\beta'' * |V_{\text{probe}} - V_{\text{probe},b}|^n), \quad (12)$$

where  $K''$ ,  $\beta''$ ,  $V_{\text{probe},b}$ , and  $n$  are all fit parameters. This form is then used in the same manner as the Gaussian fit to obtain profiles for each species peak (see Fig. 5). While this fit does not perfectly match each peak (in particular  $\text{Xe}^+$ ), it nevertheless does an excellent job capturing the overlap between each peak. This function is thus considered the most rigorous fitting method of the four investigated at the cost of added complexity.

## IV. CHARGE-EXCHANGE CORRECTION METHODS

In order to obtain accurate current and species fractions from an  $E \times B$  probe, one must also consider the effects of CEX collisions between beam ions and background neutrals. The presence of neutrals, either from the thruster mass flow or facility pumping limitations, can cause beam ions to become fast-moving neutrals via CEX collisions on their way to the  $E \times B$  probe entrance. This causes the amount of ions to become attenuated at the probe; and since the effect of CEX collisions differs for each charge species, the relative population measured at the probe can differ significantly from the population that exits the thruster. Hall thrusters are especially sensitive to this effect compared to ions thrusters due to lower discharge voltages (and thus lower ion energies), as well as typically higher mass flow rates, which lead to larger facility backpressures (see Fig. 6). Plume attenuation due to CEX loss was neglected in Refs. 1, 4, 13, and 14



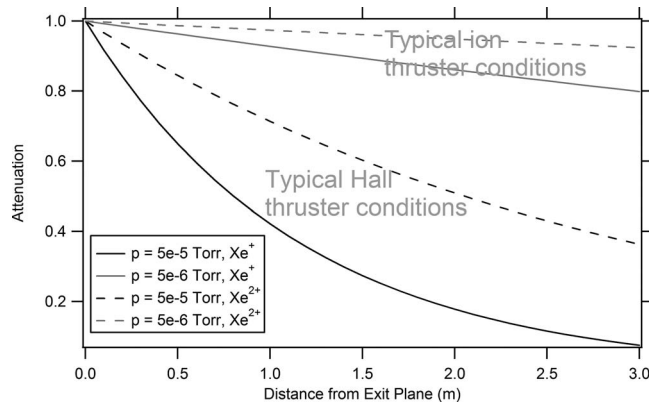
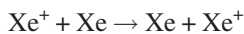


FIG. 6. Comparison of beam attenuation due to CEX effects for singly and doubly ionized xenon as a function of probe distance. Note that the larger backpressures for Hall thruster operation cause a much more severe CEX loss.

that may have impacted the reported ion species fractions, but will not be considered here. The method of correcting for CEX collisions on the measured charge state is discussed below.

### A. Baseline CEX correction model

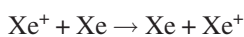
A CEX model for ion thrusters, derived by Anderson,<sup>15</sup> is employed and simplified in this investigation. This model assumes a one-dimensional beam consisting of ions all accelerated by the same potential, traveling through a uniform neutral background of density  $n_0$ . The relevant set of CEX reactions taken into account in Anderson's model are



$$\text{(at singly ionized xenon energy, cross section } \sigma_1), \quad (13a)$$



$$\begin{aligned} &\text{(one at doubly ionized xenon energy,} \\ &\text{one at thermal energy, cross section } \sigma_3), \quad (13c) \end{aligned}$$



$$\text{(at doubly ionized xenon energy, cross section } \sigma_4). \quad (13d)$$

Equation (13c) is regarded as an asymmetric reaction, since a new type of ion (in this case,  $\text{Xe}^+$ ) is created in the collision. All other reactions above are termed symmetric reactions. Cross sections are taken from Miller *et al.*,<sup>16</sup> which are empirical fits to experimental data

$$\sigma_1, \sigma_4: \sigma = 87.3 - 13.6 \log(E), \quad (14a)$$

$$\sigma_2 = 45.7 - 8.9 \log(E), \quad (14b)$$

$$\sigma_3 = 2, \quad (14c)$$

where  $E$  is the ion energy in eV and all cross sections are in  $\text{\AA}^2$  ( $10^{-20} \text{ m}^2$ ). The third cross section varies only slightly over a wide range of energies, and thus was taken to be

constant. Using the standard equations for a flux of particles traveling through a stationary background gas

$$\vec{\nabla} \cdot \vec{j}_1 = -\vec{j}_1 n_0 \sigma_1, \quad (15a)$$

$$\vec{\nabla} \cdot \vec{j}_2 = -\vec{j}_2 n_0 (\sigma_2 + \sigma_3), \quad (15b)$$

$$\vec{\nabla} \cdot \vec{j}_3 = -\vec{j}_3 n_0 \sigma_4 + \frac{\vec{j}_2}{2} n_0 \sigma_3, \quad (15c)$$

where  $j_1$  is  $\text{Xe}^+$  current density (at  $\text{Xe}^+$  energy),  $j_2$  is  $\text{Xe}^{2+}$  current density, and  $j_3$  is  $\text{Xe}^+$  current density (at  $\text{Xe}^{2+}$  energy). Assuming a one-dimensional beam, Anderson found:

$$j_1 = j_{10} \exp[-n_0 \sigma_1 z], \quad (16a)$$

$$j_2 = j_{20} \exp[-n_0 (\sigma_2 + \sigma_3) z], \quad (16b)$$

$$j_3 = j_{20} \frac{\sigma_3}{2} \left\{ \frac{\exp[-n_0 \sigma_4 z] - \exp[-n_0 (\sigma_2 + \sigma_3) z]}{\sigma_2 + \sigma_3 - \sigma_4} \right\}, \quad (16c)$$

$$(j/j_0)_{\text{Xe}^+} = j_1/j_{10}, \quad (16d)$$

$$(j/j_0)_{\text{Xe}^{2+}} = \frac{j_2 + j_3}{j_{20}}. \quad (16e)$$

Thus, Eqs. (16a)–(16e) can be used with measured currents to determine the original current values at the thruster exit and therefore correct for CEX within the plume. The background gas density can be found using a facility pressure measurement. The symmetric CEX reaction between  $\text{Xe}^{3+}$  and background neutrals can easily be added to this model, if it is assumed that any asymmetric reactions involving  $\text{Xe}^{3+}$  can be neglected

$$(j/j_0)_{\text{Xe}^{3+}} = \exp[-n_0 \sigma_5 z], \quad (17a)$$

$$\sigma_5 = 16.9 - 3.0 \log(E). \quad (17b)$$

The cross section  $\sigma_5$  is provided by Dressler from Hanscom AFB<sup>17</sup> and is derived from a modified Rapp–Francis CEX 1-electron model. Any calculations regarding  $\text{Xe}^{4+}$  have been neglected since it typically comprises less than 0.1% of the beam.<sup>1</sup>

In the remainder of this section, a number of assumptions and simplifications to the above model are investigated and validated. These include the neglect of a higher neutral density near the thruster exit; assuming the effect of asymmetric reactions is small and thus negligible; eliminating the CEX correction for  $\text{Xe}^{3+}$ ; and assuming the acceleration voltage is equal to the discharge voltage in the CEX cross section calculations.

### B. Assumption of uniform neutral density field

The model outlined in Sec. III A assumes that the ion beam becomes attenuated by a neutral background gas of uniform density. While this is a reasonable assumption for the background gas caused by facility pumping limitations, the neutral density is much higher near the thruster exit due to propellant mass flow from the thruster channel. If the neutral density field  $n(z)$  is assumed to be a superposition of the

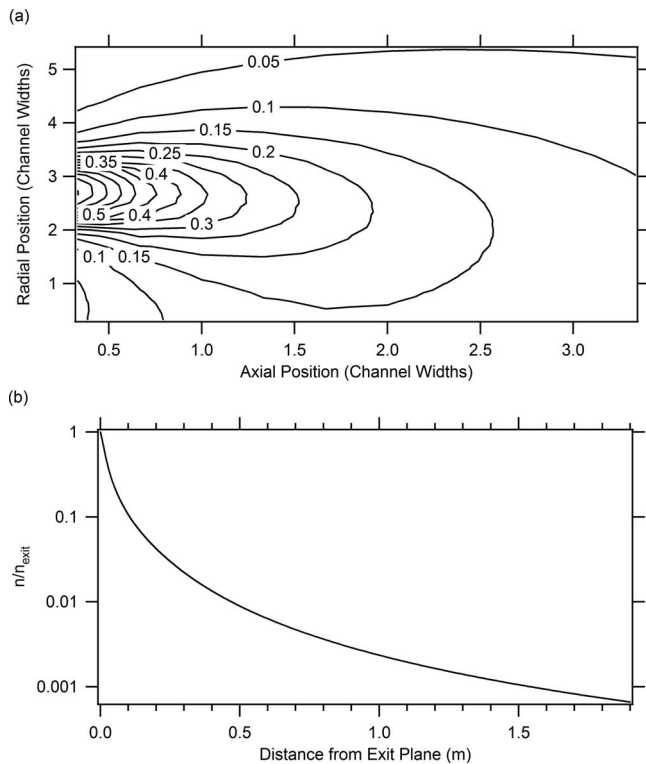


FIG. 7. Calculated density decay of thruster neutrals in the plume of a Hall thruster. *R-Z* contour plot is shown in (a). Density decay with axial position is shown in (b) at channel centerline. Both plots are normalized with respect to density at  $z=0$ .

uniform facility density  $n_o$  and the density field caused by the thruster neutral flux  $n_{th}(z)$  then the attenuation fraction can be written as

$$(j/j_o) = \exp\left[-\sigma \int n_{th}(z) dz\right] \exp(-\sigma n_o z) = \left(\frac{j_1}{j_o}\right) \left(\frac{j}{j_1}\right). \tag{18}$$

In Eq. (18),  $j_1/j_o$  is the attenuation fraction if there were no facility neutrals, i.e.,  $n_o=0$ . Thus,  $j_1$  would be the measured current at the probe if there were no facility effects. It can be argued that if a uniform background density is assumed, then only the CEX with background neutrals will be corrected. Depending on the desired measurement, it may or may not be appropriate to correct for CEX with the thruster neutral flux.

In order to estimate the relative attenuation caused by thruster neutrals when compared to the attenuation by facility neutrals, two different methods are employed. The first utilizes an analytical model of neutral flow derived by Katz.<sup>18</sup> This model provides the neutral density decay as a function of distance from the thruster exit,  $z$ , all normalized to the value at  $z=0$ . This falloff is shown in Fig. 7, as a two-dimensional contour plot and a one-dimensional curve taken at channel centerline.

A comparison was made using values for the operating condition at 300 V and 20 A. A neutral density at thruster exit was estimated using the measured anode mass flow, an assumed mass utilization efficiency of 90% (Ref. 19) and a wall temperature of 575 °C. The calculated neutral density

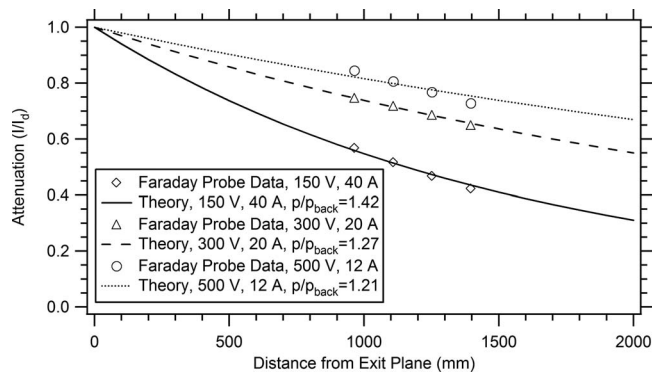


FIG. 8. Comparison of Faraday probe data to theoretical values calculated using the CEX attenuation model. Note the relative agreement between the required backpressure to fit the experimental data and the measured backpressure ( $p/p_{back}$ ).

at the thruster exit plane was found to be approximately three times larger than the measured facility background density. However, due to the rapid decay of neutral density leaving the thruster, the attenuation fraction from thruster neutrals is only 0.96, while the fraction caused by facility neutrals is 0.60. This indicates that the CEX effects from thruster neutrals are an order of magnitude smaller than those caused by facility neutrals.

The importance of correcting for CEX with thruster neutrals was also investigated using Faraday probe traces taken at various distances from the thruster. Each of these traces were integrated over radial space and plotted as a function of  $z$  as a measure of attenuation. As an estimate, the integrated currents were normalized by the discharge current for each operating condition. In order to properly compare these values to ones calculated by the CEX correction model, each species’ current must be summed. It can be shown that

$$\frac{I(z)}{I_o} = \sum \Omega_{i,o} \exp(-\bar{n}\sigma_i z). \tag{19}$$

Backpressure (or rather, “average neutral density”) was iterated until a self-consistent solution was found that yielded the proper initial current fractions  $\Omega_o$  as well as properly matched the experimental Faraday probe data. This pressure was then compared to the measured backpressure as a metric of how well the facility neutral density describes CEX attenuation (see Fig. 8).

Figure 8 shows that the required backpressure to properly describe current attenuation is always higher than the measured facility pressure. The difference, however, decreases significantly as the actual amount of CEX decreases (at higher voltages and lower currents which causes lower backpressures). It should also be noted that there are sources of error with this comparison. First, all currents were normalized by discharge current, when they should have been normalized by ion beam current at the exit plane. Second, the Faraday probe traces were taken radially and thus did not likely capture the total beam current at each axial location, especially at 150 V and 40 A. This would likely cause a larger attenuation to appear than what is caused purely by CEX, as less of the beam would be captured farther away from thruster exit. Lastly, the backpressure measurement,

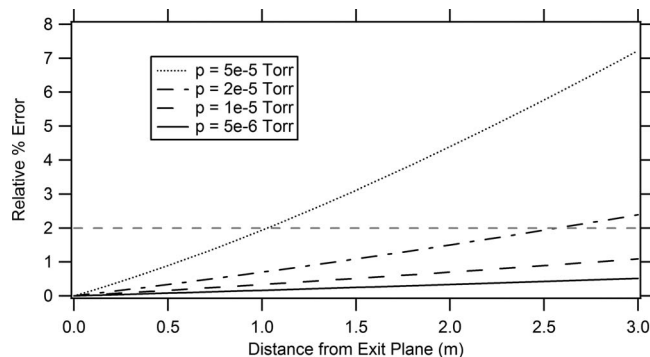


FIG. 9. Relative error induced by neglecting the asymmetric reaction in correcting for charge exchange.

taken with an ionization gauge, has an inherent 20% uncertainty. Considering these sources of error, the agreement between required and measured backpressure is quite good, and thus further evidence that CEX effects from thruster neutrals are negligible.

It should be noted that there may be circumstances where the effects of CEX caused by thruster neutrals are non-negligible. For example, if a probe were placed within a few thruster diameters of the exit plane, attenuation from thruster neutrals would dominate over attenuation from facility neutrals, and thus will likely need to be accounted for. However, for  $E \times B$  probes typically placed several diameters downstream of the exit plane, the amount of CEX caused by thruster neutrals is equivalent to that caused by facility neutrals at a backpressure of  $\sim 10^{-6}$  torr, indicating that its effects can be neglected under most situations.

### C. Importance of asymmetric reactions

Asymmetric reactions involve the creation of charge states different from the reactants. From Eqs. (14a)–(14c), it is evident that at moderate discharge voltages (hundreds of volts), the asymmetric cross section  $\sigma_3$  is smaller than the symmetric cross sections by at least an order of magnitude. This indicates that the asymmetric reaction occurs far less frequently than the other CEX reactions, and yet is a source of added complexity to the CEX correction. Thus, it is worthwhile to determine the relative error in neglecting the asymmetric reaction. This is easily accomplished by setting  $\sigma_3=0$  and comparing this simplified attenuation fraction to the complete one. Figure 9 shows the relative error in attenuation fraction for various probe distances and pressures (an acceleration voltage of 300 V was assumed).

The error created by neglecting the asymmetric reaction is shown to be less than 2%, except at large backpressures and probe distances. For typical  $E \times B$  probe applications, probe locations are 1–2 m away and the operating pressure is about  $10^{-5}$  torr, making the error less than 1%. Therefore, except under the special circumstances mentioned above, eliminating the asymmetric reaction from the CEX correction model will introduce negligible error. However, for very large backpressures and/or probes positioned very far from the thruster, asymmetric reactions should be included in the CEX correction.

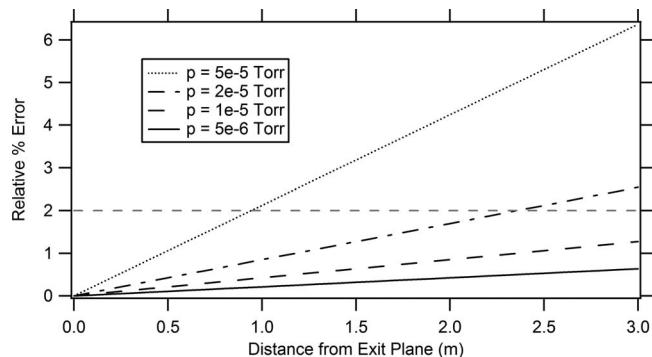


FIG. 10. Error induced by assuming acceleration voltage is equal to discharge voltage in CEX cross section equations. Cross section used was symmetric  $\text{Xe}^+$  reaction with background gas, with  $\eta_v=0.8$ .

While this in itself does not greatly reduce the complexity of the model, if we also assume that other asymmetric reactions are infrequent enough to be neglected, then the symmetric reaction of  $\text{Xe}^{3+}$  with background neutrals can be confidently included without the need for several additional reactions. This addition, however, has little effect on species fractions due to its small cross section. We find that across all operating conditions investigated, the relative change in  $\text{Xe}^+$  and  $\text{Xe}^{2+}$  species fraction was less than 0.15%, and the relative change in  $\text{Xe}^{3+}$  was less than 20%. Despite this small effect, the correction for  $\text{Xe}^{3+}$  was left in the final CEX model for completeness (see Sec. IV E).

### D. Cross section sensitivity to ion energy

In order to calculate the CEX cross sections within the model, the relevant ion energy must be known. While this value is easily determined for ion thrusters, the acceleration voltage in Hall thrusters differs from the applied discharge voltage and must be measured, usually with a retarding potential analyzer (RPA). However, it is impractical to require the use of an RPA for every  $E \times B$  probe measurement. Since the cross sections are only weakly dependent on ion energy, the error in assuming the acceleration voltage is equal to the discharge voltage was investigated. Given the general cross section formula  $\sigma = a_1 - a_2 \log(E)$ , and defining the relative error as

$$\varepsilon = \frac{(j/j_0)_{V_d} - (j/j_0)_{V_a}}{(j/j_0)_{V_a}}, \quad (20)$$

one can show, assuming that  $\varepsilon \ll 1$ , that

$$\varepsilon \approx \frac{a_2 p z}{kT} \log\left(\frac{1}{\eta_v}\right), \quad (21)$$

where  $p$  is the backpressure,  $\eta_v$  is the voltage utilization efficiency,  $V_a/V_d$ , and the rest of the symbols have their usual meaning. Figure 10 plots this error as a function of backpressure and probe distance, using the  $\text{Xe}^+$  CEX cross section and assuming  $\eta_v=0.8$  (to maximize possible error):

For typical conditions of 1–2 m probe position and  $10^{-5}$  torr, the error created is well within 1%. Noting that this is likely the worst case, it is reasonable (and also practical) to use the discharge voltage to calculate the relevant ion energies in the CEX correction model.

TABLE I. List of Hall thruster operating conditions investigated.

Discharge voltage (V)	Discharge current (A)	Cathode mounting location
150	40	Internal
300	20	Internal
500	12	Internal
300	10	Internal
150	40	External
300	20	External
500	12	External
300	10	External

### E. Simplified CEX correction model

The final CEX correction model used in this investigation is summarized here. This model only corrects for symmetric reactions between ions and a uniform neutral background density, which is calculated using a facility pressure measurement. It also assumes an acceleration voltage equal to the discharge voltage when calculating ion energies. This allows for a simple yet reasonably accurate method of correcting for CEX within the plume. The final equations are

$$(j/j_0)_{Xe^+} = \exp(-n_0\sigma_1z) \quad \sigma_1 = 87.3 - 13.6 \log(V_d), \quad (22)$$

$$(j/j_0)_{Xe^{2+}} = \exp(-n_0\sigma_2z) \quad \sigma_2 = 45.7 - 8.9 \log(2V_d), \quad (23)$$

$$(j/j_0)_{Xe^{3+}} = \exp(-n_0\sigma_3z) \quad \sigma_3 = 16.9 - 3.0 \log(3V_d). \quad (24)$$

## V. RESULTS

An  $E \times B$  probe was placed on centerline 1.9 m downstream of a 6 kW laboratory Hall thruster, and used to measure the charge state population at eight different operating conditions (see Table I). In Table I, internal cathode mounting refers to a location on thruster centerline, while external cathode mounting is outside the outer diameter of the magnetic circuit. Each of these data sets was analyzed using the methods outlined in Secs. III and IV E. In order to more fully characterize the effects of correcting for charge exchange, three levels of correction were used: no CEX correction, correcting only the  $Xe^+$  population for CEX, which should be the most significant correction, and correcting all three species for CEX. These three levels of correction, in addition to the four methods of including species' peak width, provided twelve different methods of analysis for comparison. Due to similarity in trends across several operating conditions, only the four with the internally mounted cathode are presented here.

Variations in species fractions, along with the relevant performance parameters  $\sum \Omega_i/Z_i$  and  $\sum \Omega_i/\sqrt{Z_i}$  (Ref. 4) were investigated across analysis methods. However, the performance parameters allow for a compact method of presenting the charge state that would otherwise have to be described with three species fractions. Furthermore, the variation in the performance parameters is of greater interest as these quantities are ultimately used in the determination of thruster ef-

iciency. In particular, the anode efficiency for a Hall thruster can be decomposed into the product of several utilization efficiencies given as<sup>20</sup>

$$\eta_a = \eta_q \eta_v \eta_d \eta_b \eta_m = \frac{(\sum \Omega_i/\sqrt{Z_i})^2}{\sum \Omega_i/Z_i} \left(1 - \frac{V_l}{V_d}\right) \times (\cos \theta)^2 \left(\frac{I_b}{I_d}\right)^2 \left(\frac{m_{Xe} J_d}{\dot{m}_a e}\right) \sum \frac{\Omega_i}{Z_i}. \quad (25)$$

The terms directly affected by the presence of multiply charged ions are the charge utilization efficiency and the mass utilization efficiency, given by

$$\eta_q = \frac{(\sum \Omega_i/\sqrt{Z_i})^2}{\sum \Omega_i/Z_i}, \quad (26)$$

$$\eta_m = \left(\frac{m_{Xe} J_d}{\dot{m}_a e}\right) \left(\frac{I_b}{I_d}\right) \sum \frac{\Omega_i}{Z_i} = \left(\frac{m_{Xe} J_d}{\dot{m}_a e}\right) \left(\frac{I_b}{I_d}\right) \alpha_m. \quad (27)$$

Therefore, variations in  $\eta_q$  and  $\alpha_m$  are considered to have a direct correlation with variations in the calculated thruster efficiency. Since it was found that  $\alpha_m$  varied more significantly than  $\eta_q$  over all test cases, only variations in  $\alpha_m$  are presented here. The effective charge state  $Q$ , defined as  $\sum \zeta_i Z_i$ , is another relevant parameter when discussing the charge state population;<sup>21</sup> however, since it has no direct impact on the calculation of efficiency in the above model, it is not presented in detail here.

The purpose of such a comparison across analysis methods is to quantify the importance of correcting for peak width and CEX in determining current and species fractions, and thus propose a method that yields the best balance of accuracy and simplicity. Since the most complex method, and arguably the most accurate, is the variable exponential fit with full CEX correction, all methods are compared relative to this one. Thus, all results will be presented in terms of relative percent difference between  $\alpha_m$  for each method and  $\alpha_m$  for the most complex method. Results across four operating conditions are presented below.

### A. Operating condition of 150 V, 40 A

This particular condition of low voltage and high current represents a case of potentially large amounts of CEX collisions within the plume. Facility pressure was measured to be  $2.6 \times 10^{-5}$  torr, corrected for xenon. The variation in  $\alpha_m$  with each analysis method is shown in Fig. 11.

From Fig. 11 it is evident that the effects of correcting for CEX dominate over the effects of peak width, as expected. Relative errors reached as high as almost 8%, which is extremely significant in the context of efficiency analysis. Once the full CEX correction is applied, the relative error drops to nearly within 1%, regardless of which method is used to include peak width. It is interesting to note that the error induced from correcting for peak width but not CEX is larger than correcting for nothing at all. This is a characteristic that will be shown at other operating conditions as well.



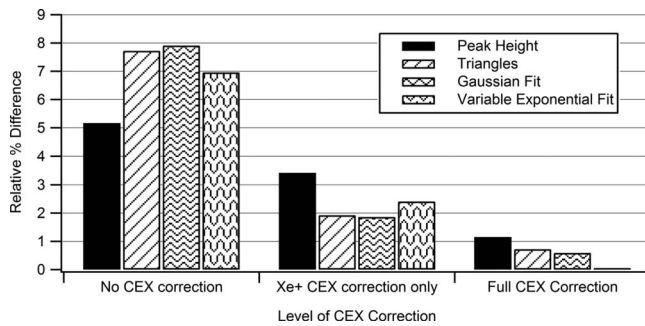


FIG. 11. Comparison of  $\alpha_m$  between several analysis methods at 150 V, 40 A, relative to the full CEX correction using the variable exponential fit. Notice the dominance of the effects of CEX correction over the differences in peak width methods.

### B. Operating condition of 300 V, 20 A

This particular condition of moderate voltage and current represents a more typical case of Hall thruster operation. Facility pressure was measured to be  $1.6 \times 10^{-5}$  torr, corrected for xenon. The variation in  $\alpha_m$  with each analysis method is shown in Fig. 12.

The most noticeable feature at this operating condition is that the relative error is maximized when either peak width OR CEX collisions are corrected for. As with the data at 150 V, 40 A, there is negligible difference between any method that takes peak width into account. Relative difference is minimized to within 0.1% using a full CEX correction and any method including peak width. It is interesting to note that at this particular operating condition, using peak heights and not correcting for CEX gave a nearly identical result to the variable exponential fit with full CEX correction method. This can be explained by noting that the two correction factors have opposite effects on the calculated charge state. As peaks tend to be wider for higher charge states, including them shifts the overall charge state to a larger value. Conversely, CEX affects  $Xe^+$  more than higher charge states, so correcting for this shifts the charge state closer to one. These two competing effects give the interesting result that correcting for either peak width or CEX will typically yield a higher difference than correcting for nothing at all using the simplest method.

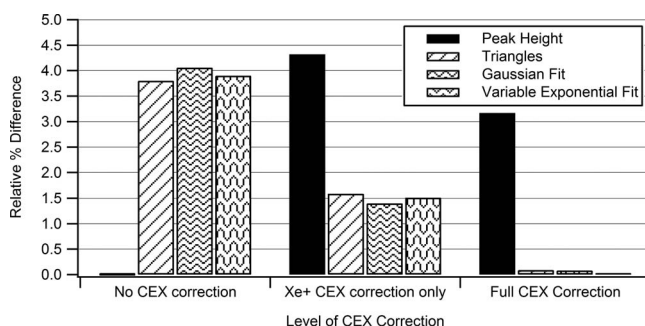


FIG. 12. Comparison of  $\alpha_m$  between several analysis methods at 300 V, 20 A, relative to the full CEX correction using the variable exponential fit. Notice that the largest errors occur from correcting for either CEX or peak width.

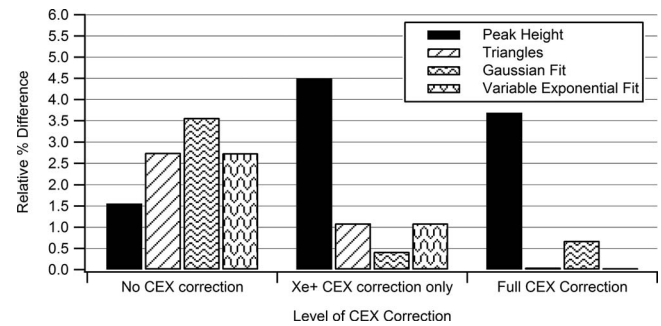


FIG. 13. Comparison of  $\alpha_m$  between several analysis methods at 500 V, 12 A, relative to the full CEX correction using the variable exponential fit.

### C. Operating condition at 500 V, 12 A

The particular condition of higher voltage and lower current is a case where a much smaller amount of CEX likely occurs within the plume. Facility pressure was measured to be  $1.2 \times 10^{-5}$  torr, corrected for xenon. The variation in  $\alpha_m$  with each analysis method is shown in Fig. 13.

As with 300 V and 20 A, the largest differences occur when either peak width or CEX is corrected for but not the other. In order for the relative difference to be within 1%, only a full CEX correction along with any inclusion of peak width is sufficient. This trend is present in all operating conditions investigated.

### D. Operating condition at 300 V, 10 A

This condition was taken at a discharge power that is half of the power of the other test cases. The discharge current is also the lowest investigated, with a facility pressure measured to be  $9.7 \times 10^{-6}$  torr, corrected for xenon. The variation in  $\alpha_m$  with each analysis method is shown in Fig. 14.

This particular case shows the lowest relative differences calculated, with a maximum of only 2.5%. Once again, the maximum differences occur when either peak widths or CEX are accounted for. At this particular pressure, it appears that only a correction to  $Xe^+$  with an inclusion of peak width is required to be within 1% of the variable exponential fit and full CEX correction method. This indicates that the correction of CEX for higher charge states is less significant at lower pressures, which is to be expected.

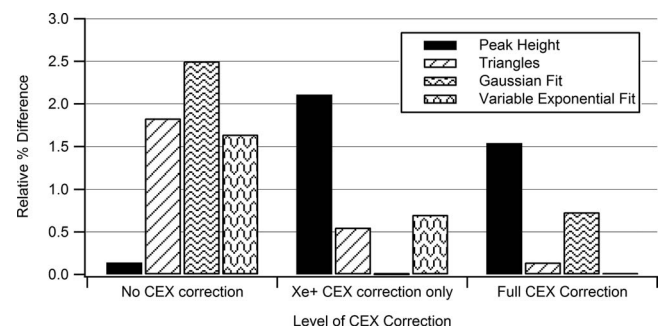


FIG. 14. Comparison of  $\alpha_m$  between several analysis methods at 300 V, 10 A, relative to the full CEX correction using the variable exponential fit.

## VI. DISCUSSION

Based on the results from the eight different operating conditions investigated, it is recommended that the method of triangle fitting with the full CEX correction be used to analyze  $E \times B$  probe spectra from Hall thruster plumes. Results from this method are consistently within 1% of the results from the most complex method used over a wide range of operating conditions. It has been shown that correcting for CEX can yield a significantly different charge state, especially at high facility pressures, while the triangle fitting method provides effectively the same results when compared to higher order fit methods. Thus, this method provides the best balance between simplicity and accuracy over all operating conditions investigated. It should be noted that the method of triangle fitting is sufficient merely in calculating current and species fractions; this approximation does not capture much of the detail of each species peak, and therefore should not be used for analyzing the physics of the VDF.

In order to prevent facility effects from excessively altering the  $E \times B$  probe measurement, it is recommended that the attenuation fraction of  $\text{Xe}^+$  be kept above 0.7. While this is an arbitrary choice, it provides a reasonable guideline for controlling the magnitude of CEX effects within the plume. Since the CEX cross section of  $\text{Xe}^+$  with neutrals is only weakly dependent on ion energy, this attenuation fraction guideline can be roughly converted into a  $pz$  factor of backpressure multiplied by probe distance from the exit plane, which is more practical. Thus, in order to keep facility effects at a reasonable level, it is recommended that  $pz \leq 2$ , where  $p$  is the facility backpressure in units of  $10^{-5}$  torr, and  $z$  is the distance from the thruster exit plane to the  $E \times B$  probe in meters. In this study,  $pz$  varied between 1.8 at 10 A and 4.9 at 40 A. While the above recommendation was not strictly met,  $pz$  was still kept at a reasonable level for all operating conditions except 40 A, and therefore the results presented above are considered valid. A study performed by Reid *et al.*<sup>9</sup> utilized the above methods on  $E \times B$  probe spectra taken at various distances from the thruster. After correction, excellent results were obtained that were consistent across all distances tested, providing further validation of the recommended analysis method.

### A. Error analysis

Each analysis method investigated above provides a certain amount of additional uncertainty in the calculated charge state, due to the larger amount of data processing required. Major sources of uncertainty include the facility pressure measurement, estimated at 20%, the cross sections within the CEX correction model, estimated at 20% for  $\text{Xe}^+$  and 30% for  $\text{Xe}^{2+}$  and  $\text{Xe}^{3+}$ , and each fitting method. Taking into account uncertainties in pressure and cross sections, the CEX correction generates an additional relative uncertainty of up to 2%–8% in  $\text{Xe}^+$  current fraction, 15%–50% in  $\text{Xe}^{2+}$  current fraction, and 10%–30% in  $\text{Xe}^{3+}$  current fraction. This corresponds to an additional relative uncertainty of up to 1%–4% for  $\alpha_m$ . It should be noted that the quantities calculated without the CEX correction always lay outside these uncertainty bounds, indicating that the correction is still certainly worth

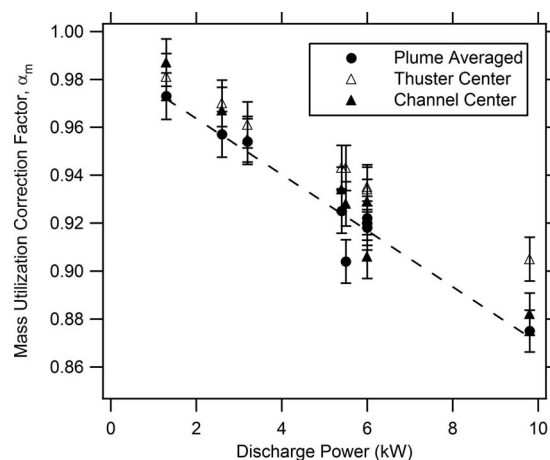


FIG. 15. Comparison of  $\alpha_m$  calculated from a thruster centerline, channel centerline, and plume-averaged measurement, as a function of discharge power. Error bars are 1%. (From Ref. 9.)

doing. Also, the amount of uncertainty is directly related to the facility pressure, and consequently the amount of CEX within the plume. Therefore, a lower backpressure will result in smaller uncertainty bounds created by the CEX correction.

Errors induced by using the triangle fitting method can be estimated by comparing calculated values between this method and the more rigorous variable exponential fit method. The relative amount of error was found to be up to 2.5% for  $\text{Xe}^+$  current fraction, 20% for  $\text{Xe}^{2+}$  current fraction, and 25% for  $\text{Xe}^{3+}$  current fraction, corresponding to errors of up to 1% for  $\alpha_m$ . Noting that all of above estimates are maximum deviations, the combined standard uncertainty has been estimated as 3% in  $\text{Xe}^+$ , 20% in  $\text{Xe}^{2+}$  and  $\text{Xe}^{3+}$ , and 2% in  $\alpha_m$ .

### B. Species fraction spatial dependence

While the above described methods are applicable to an  $E \times B$  probe spectrum taken anywhere in the plume, measurements are typically taken along thruster centerline 1–2 m downstream of the exit plane. In order to characterize the species population within the plume, one must consider any spatial variation which occurs and its effect on the overall charge state. Experiments performed by Kim<sup>1</sup> and simulations performed by Katz<sup>22</sup> on the SPT-100 have shown that species fractions can vary significantly off-centerline, showing that there is a larger population of multiply charged species farther off axis. This indicates that a single-point centerline measurement may not be sufficient to describe accurately the average charge state of ions exiting the thruster.

Experiments performed by Reid *et al.*<sup>9</sup> on a 6 kW laboratory Hall thruster verifies the existence of higher charge states off thruster centerline. An average  $\alpha_m$  was found over the spatial domain tested, weighted by the local current density, and compared to the values yielded by the thruster centerline and channel centerline measurements (see Fig. 15). This average varied up to 3.5% from the single-point thruster centerline measurement, but only by 1.5% when compared to the single-point channel centerline measurement. It was thus suggested that a measurement taken at channel centerline

would be sufficient for studies concerned with thruster behavior over large throttling ranges, with appropriate error bounds to accommodate the spatial variation within the plume. However, for studies focused on fine changes in thruster performance, the resulting error in a single-point measurement may not be tolerable and determining plume-averaged quantities will be necessary.

## VII. CONCLUSION

Various analysis methods were applied to  $E \times B$  probe spectra taken in the plume of a 6 kW laboratory Hall thruster over a wide range of operating conditions. These methods incorporated varying degrees of correction for the width of species peaks as well as CEX collision effects within the plume, in order to determine the importance of these effects on the calculated species fractions and efficiency terms. It has been shown that the use of a simple model using triangles to approximate the velocity distribution function for each species peak is sufficient to capture the effect of peak width on calculated species fraction. While the extent of CEX varies strongly with the facility backpressure, it has been found that the effects of CEX are extremely significant at pressures larger than  $10^{-5}$  torr, and thus should be corrected for. However, a simplified method of correction has been suggested that can easily be implemented and generate small uncertainty over the majority of cases. Most importantly, it has been shown that the amount of CEX caused by the neutral thruster flux (as opposed to facility neutrals) is negligible except when the probe is very close to the exit plane (a few thruster diameters). In order to keep the amount of CEX within reasonable limits, it is recommended that the product of  $p$  and  $z$  be kept below two, where  $p$  is the facility pressure in units of  $10^{-5}$  torr, and  $z$  is the distance from thruster exit to the probe in meters. Lastly, it has been suggested by Reid *et al.*<sup>9</sup> that a single-point measurement at thruster centerline is insufficient to properly characterize the charge state of the thruster plume. However, a single-point measurement taken at channel centerline can minimize the error to within 1.5% when compared to the average of a more complete spatial map. The methods suggested in this paper should allow for a more accurate determination of the charge state of Hall thruster plumes, and thus facilitate a more accurate understanding of the competing processes affecting overall thruster efficiency.

## ACKNOWLEDGMENTS

The authors would like to thank John Anderson and Ira Katz at JPL for their assistance on formulation and development of the charge exchange correction model used in this paper, along with Rainer Dressler at Hanscom AFB for providing additional xenon charge exchange cross sections. The research described in this paper was carried out at the Jet Propulsion Laboratory, California Institute of Technology, under a contract with the National Aeronautics and Space Administration. The leading author is supported under the Graduate Student Research Program through the National Aeronautics and Space Administration.

- <sup>1</sup>S.-W. Kim, Ph.D. thesis, University of Michigan, 1999.
- <sup>2</sup>S.-W. Kim and A. D. Gallimore, *J. Spacecr. Rockets* **39**, 904 (2002).
- <sup>3</sup>L. B. King and A. D. Gallimore, *J. Propul. Power* **16**, 1086 (2000).
- <sup>4</sup>R. R. Hofer, Ph.D. thesis, The University of Michigan, 2004.
- <sup>5</sup>R. R. Hofer and A. D. Gallimore, *J. Propul. Power* **22**, 732 (2006).
- <sup>6</sup>E. Leal-Quiros and M. A. Prelas, *Rev. Sci. Instrum.* **60**, 350 (1989).
- <sup>7</sup>E. L. Quiros, *J. Appl. Phys.* **52**, 1152 (1981).
- <sup>8</sup>R. L. Seliger, *J. Appl. Phys.* **43**, 2352 (1972).
- <sup>9</sup>B. M. Reid, R. Shastry, A. D. Gallimore, and R. R. Hofer, *Proceedings of the 44th AIAA/ASME/SAE/ASEE Joint Propulsion Conference and Exhibit*, Hartford, CT (AIAA, Reston, VA, 2008).
- <sup>10</sup>J. R. Anderson and D. Fitzgerald, *Proceedings of the 32nd AIAA/ASME/SAE/ASEE Joint Propulsion Conference and Exhibit*, Lake Buena Vista, FL (AIAA, Reston, VA, 1996).
- <sup>11</sup>A. Sengupta, J. R. Brophy, J. R. Anderson, C. Garner, B. Banks, and K. de Groh, *Proceedings of the 40th AIAA/ASME/SAE/ASEE Joint Propulsion Conference and Exhibit*, Fort Lauderdale, FL (AIAA, Reston, VA, 2004).
- <sup>12</sup>T. M. Randolph and J. E. Polk, *Proceedings of the Space 2004 Conference and Exhibit*, San Diego, CA (AIAA, Reston, VA, 2004).
- <sup>13</sup>B. E. Beal, Ph.D. thesis, University of Michigan, 2004.
- <sup>14</sup>J. A. Linnell, Ph.D. thesis, University of Michigan, 2007.
- <sup>15</sup>J. Anderson, "Charge-exchange collision effect on  $E \times B$  probe location for NEXIS testing," Internal Memorandum, Jet Propulsion Laboratory, 16 January 2004.
- <sup>16</sup>J. S. Miller, S. H. Pullins, D. J. Levandier, Y.-h. Chiu, and R. A. Dressler, *J. Appl. Phys.* **91**, 984 (2002).
- <sup>17</sup>R. A. Dressler, personal communication (30 October 2007).
- <sup>18</sup>I. Katz, personal communication (15 November 2007).
- <sup>19</sup>K. K. Jameson, D. M. Goebel, R. R. Hofer, and R. M. Watkins, *Proceedings of the 30th International Electric Propulsion Conference*, Florence, Italy (Electric Rocket Propulsion Society, Fairview Park, OH, 2007).
- <sup>20</sup>R. R. Hofer, I. Katz, I. G. Mikellides, D. M. Goebel, K. K. Jameson, R. M. Sullivan, and L. K. Johnson, *Proceedings of the 44th AIAA/ASME/SAE/ASEE Joint Propulsion Conference and Exhibit*, Hartford, CT (AIAA, Reston, VA, 2001).
- <sup>21</sup>C. W. Larson, D. L. Brown, and W. A. Hargus, *Proceedings of the 43rd AIAA/ASME/SAE/ASEE Joint Propulsion Conference and Exhibit*, Cincinnati, OH (AIAA, Reston, VA, 2007).
- <sup>22</sup>I. Katz, R. R. Hofer, and D. M. Goebel, *IEEE Trans. Plasma Sci.* **36**, 2015 (2008).